AGU PUBLICATIONS

JGR

Journal of Geophysical Research: Space Physics

RESEARCH ARTICLE
10.1002/2014JA020678

Special Section:
Origins and Properties of Kappa Distributions

Key Points:
- Kappa distributions successfully describe plasmas out of thermal equilibrium
- A global kinetic model of the solar corona and solar wind is described
- The model is extended by incorporating azimuthally varying boundary conditions

Correspondence to:
V. Pierrard,
viviane.pierrard@oma.be

Citation:
Pierrard, V., and M. Pieters (2014), Coronal heating and solar wind acceleration for electrons, protons, and minor ions obtained from kinetic models based on kappa distributions, *J. Geophys. Res. Space Physics*, *119*, 9441–9455, doi:10.1002/2014JA020678.

Received 30 SEP 2014
Accepted 23 NOV 2014
Accepted article online 17 NOV 2014
Published online 23 DEC 2014

Coronal heating and solar wind acceleration for electrons, protons, and minor ions obtained from kinetic models based on kappa distributions

V. Pierrard[1,2] and M. Pieters[1]

[1]Belgian Institute for Space Aeronomy, STCE and Space Physics, Brussels, Belgium, [2]TECLIM, Earth and Life Institute, Université Catholique de Louvain, Louvain-La-Neuve, Belgium

Abstract Astrophysical and space plasmas are commonly found to be out of thermal equilibrium; i.e., the velocity distribution functions of their particles are not well described by Maxwellian distributions. They generally have more suprathermal particles in the tail of the distribution. The kappa distribution provides a generalization to successfully describe such plasmas with tails decreasing as a power law of the velocity. In the present work, we improve the solar wind model developed on the basis of such kappa distributions by incorporating azimuthally varying 1 AU boundary conditions to produce a spatially structured view of the solar wind expansion. By starting from the top of the chromosphere to the heliosphere and by applying relevant boundary conditions in the ecliptic plane, a global model of the corona and the solar wind is developed for each particle species. The model includes the natural heating of the solar corona automatically appearing when an enhanced population of suprathermal particles is present at low altitude in the solar (or stellar) atmosphere. This applies not only for electrons and protons but also for the minor ions which then have a temperature increase proportional to their mass. Moreover, the presence of suprathermal electrons contributes to the acceleration of the solar wind to high bulk velocities when Coulomb collisions are neglected. The results of the model are illustrated in the solar corona and in solar wind for the different particle species and can now be directly compared in two dimensions with spacecraft observations in the ecliptic plane.

1. Introduction

Nonthermal particle distributions are ubiquitous in space plasmas, their presence having frequently been confirmed by interplanetary missions. The particle velocity distribution functions in space plasmas generally show non-Maxwellian suprathermal tails decreasing as a power law of the velocity. Such distributions are well fitted by the so-called kappa distribution. *Scudder* [1992a, 1992b] was the pioneer to show the importance of these suprathermal particles in the heating of stellar atmospheres. In his two papers, *Scudder* [1992a, 1992b] defined a very interesting but controversial idea: the heating necessary to produce the steep temperature inversion in the solar transition region and corona can be achieved without any wave or magnetic energy needing to be deposited. The model developed in the present paper is based on the same concept.

Several works have been made to analyze the origin, the effects, and the consequences of the presence of nonthermal distributions (see *Pierrard and Lazar* [2010] for a review). *Scudder and Olbert* [1979] already demonstrated that Coulomb collisions determine the population and shape of both the thermal and suprathermal electron regimes. Recent advances in space physics show that empirical kappa distributions naturally emerge from statistical mechanics and thermodynamics [*Livadiotis and McComas*, 2010]. Generalizations of thermodynamics based on the Tsallis nonextensive entropy formalism have shown that the kappa distributions result from a new generalized Lorentzian statistical mechanics formulated for a collisionless plasma far from thermal (Maxwell–Boltzmann) equilibrium but containing turbulence in quasi-stationary equilibrium [*Livadiotis and McComas*, 2011]. In any case, the presence of such distributions in many different space plasmas suggests a universal mechanism for the creation of such suprathermal tails. Turbulence can play a role in the generation of such suprathermal tails, as well as the long-range correlations supplied by the field and plasma instabilities [*Pierrard et al.*, 2011]. Due to the properties of

the Coulomb collisions, the energetic particles are noncollisional even when thermal particles are submitted to collisions [*Pierrard*, 2012a].

The enhanced population of energetic particles plays a crucial role in the heating and acceleration of plasma in several important space and astrophysical contexts. They contribute to the heat flux and modify the classical Spitzer–Harm expression [*Pierrard*, 2012b]. They have important consequences concerning the temperature increase in the stellar, solar, and planetary atmospheres, as well as concerning the acceleration of the solar wind particles [*Scudder*, 1992a, 1992b]. Such consequences are well evidenced by using kappa distributions in kinetic models, where no closure requires the distributions to be nearly Maxwellians [*Pierrard*, 2012c]. Such models have been developed and applied to the ion-exospheres [*Pierrard and Lemaire*, 1996], the solar wind [*Maksimovic et al*., 1997a; *Zouganelis et al*., 2003], the solar corona [*Pierrard and Lamy*, 2003], the terrestrial ionosphere and plasma sheet [*Khazanov et al*., 1998], the polar wind of the Earth [*Pierrard and Lemaire*, 2001; *Tam et al*., 2007] and other planets like Jupiter and Saturn [*Pierrard*, 2009], some satellites like the Io torus [*Meyer-Vernet et al*., 1995], the terrestrial auroral regions [*Pierrard et al*., 2007], the plasmasphere [*Pierrard and Borremans*, 2012a], and the radiation belts [*Pierrard and Borremans*, 2012b] among many others. They have been generalized to arbitrary potential energy distributions [*Liemohn and Khazanov*, 1998; *Lamy et al*., 2003]. Suprathermal electrons generate large ambipolar electric fields along open magnetic flux tubes in stellar coronae and in planetary ionospheres and thus contribute significantly to solar and stellar wind accelerations, outflow from planetary ionospheres, and possibly even exoplanetary atmospheric loss.

2. Principles of the Kinetic Model

The kappa model described in the present paper is an improvement of the first kinetic exospheric model based on kappa velocity distribution functions (VDFs) developed by *Pierrard and Lemaire* [1996]. First applied to ion-exospheres in general, the model was adapted to the solar wind by *Maksimovic et al*. [1997a] and improved by *Lamy et al*. [2003] for nonmonotonic potentials. The model also includes minor ions [*Pierrard et al*., 2004].

The exospheric model starts from an altitude called the exobase, located in the solar corona, from which the solar wind begins to expand. In the present work, we start from the top of the chromosphere, considering also the region where collisions need to be taken into account, and we go to large distances in the heliosphere. We show how the characteristics of the plasma change with the distance and how the solar rotation influences the profiles.

The kinetic models provide the velocity distribution functions $f(\vec{r},\vec{v},t)$ of the particles as a solution of the evolution equation:

$$\frac{\partial f}{\partial t}+\vec{v}\cdot\frac{\partial f}{\partial \vec{r}}+\vec{a}\cdot\frac{\partial f}{\partial \vec{v}}=\left(\frac{df}{dt}\right)_c \tag{1}$$

where t is the time, $\vec{r}$ is the position, $\vec{v}$ is the velocity vector, $\vec{a}$ is the acceleration, and m is the mass of the particles. The first term of this equation represents the time dependence of the VDF and is neglected in case of steady state models as we consider here. The second term corresponds to the spatial diffusion, and the third term takes into account the effects of the external forces $\vec{F}=m\,\vec{a}$. The term in the right-hand side of the equation represents the effects of collisions and other interactions.

The calculation of the moments of the velocity distribution functions of each particle species gives the macroscopic quantities such as

1. the number density:

$$n\left(\vec{r}\right)=\int_{-\infty}^{\infty} f\left(\vec{r},\vec{v}\right)\; d\vec{v} \tag{2}$$

2. the particle flux:

$$\vec{F}\left(\vec{r}\right)=\int_{-\infty}^{\infty} f\left(\vec{r},\vec{v}\right)\;\vec{v}\;\; d\vec{v} \tag{3}$$

3. the bulk velocity:

$$\vec{u}\left(\vec{r}\right) = \frac{\vec{F}(\vec{r})}{n(\vec{r})} \tag{4}$$

4. the pressure:

$$\vec{P}\left(\vec{r}\right) = m\int_{-\infty}^{\infty} f\left(\vec{r},\vec{v}\right)\left(\vec{v}-\vec{u}\right)\left(\vec{v}-\vec{u}\right)d\vec{v} \tag{5}$$

5. the temperature:

$$T\left(\vec{r}\right) = \frac{m}{3kn(\vec{r})}\int_{-\infty}^{\infty} f\left(\vec{r},\vec{v}\right)|v-u|^2 d\vec{v} \tag{6}$$

6. the energy flux:

$$\vec{E}\left(\vec{r}\right) = \frac{m}{2}\int_{-\infty}^{\infty} f\left(\vec{r},\vec{v}\right)|v-u|^2\left(\vec{v}-\vec{u}\right)d\vec{v} \tag{7}$$

The particles are submitted to the effects of the external forces, i.e., the gravitational force, the electric force, and the Lorentz force due to the presence of the magnetic field $\vec{B}$:

$$\vec{a} = \left(\vec{g} + \frac{Ze\vec{E}}{m}\right) + \frac{Ze}{m}\left(\vec{v}\times\vec{B}\right). \tag{8}$$

Electron VDFs measured in situ in the solar wind and more generally in space plasmas are characterized by a thermal core population and a halo of suprathermal electrons [*Pierrard et al.*, 2001b]. Such distributions with suprathermal tails are well fitted by the so-called kappa or Lorentzian distributions:

$$f = \frac{n}{\pi^{3/2}}\frac{1}{\theta^3}\frac{1}{\kappa^{3/2}}\frac{\Gamma(\kappa+1)}{\Gamma(\kappa-1/2)}\left(1+\frac{v^2(r)}{\kappa\theta^2}\right)^{-\kappa-1} \tag{9}$$

where

$$\theta^2 = \frac{\kappa-3/2}{\kappa}\frac{2kT}{m} \tag{10}$$

n is the number density, T is the temperature, Γ is the gamma function, and k the Boltzmann constant (see *Pierrard and Lazar* [2010] for a review). The value of the kappa index κ determines the slope of the energy spectrum of the suprathermal electrons forming the tail of the VDF. In the limit $\kappa \to \infty$, the kappa function degenerates into a Maxwellian, for which we will present some results as well to clearly show the influence of suprathermal tails.

Using such VDF at a reference altitude and applying Liouville's theorem, we can derive the VDF of each particle species with the conservation of energy and magnetic moment [*Pierrard and Lemaire*, 1996].

3. From the Top of the Chromosphere to the Heliosphere

In the present work, we start from very low altitude, the top of the chromosphere. We consider that this level corresponds to the nonthermal limit, i.e., the altitude where the Coulomb collisions are sufficient to maintain isotropic distributions but cannot keep the plasma in thermal equilibrium. Several observations have proved that space plasmas have non-Maxwellian distributions and that kappa distributions can constitute a suitable generalization arising naturally from Tsallis statistical mechanics in case of plasmas out of thermal equilibrium [*Leubner*, 2002; *Livadiotis and McComas*, 2009]. This behavior is related to the turbulence and the long-range properties of Coulomb collisions in case of low-density plasmas [*Pierrard and Lazar*, 2010]. Because the mean free path of the charged particles increases as the fourth power of the

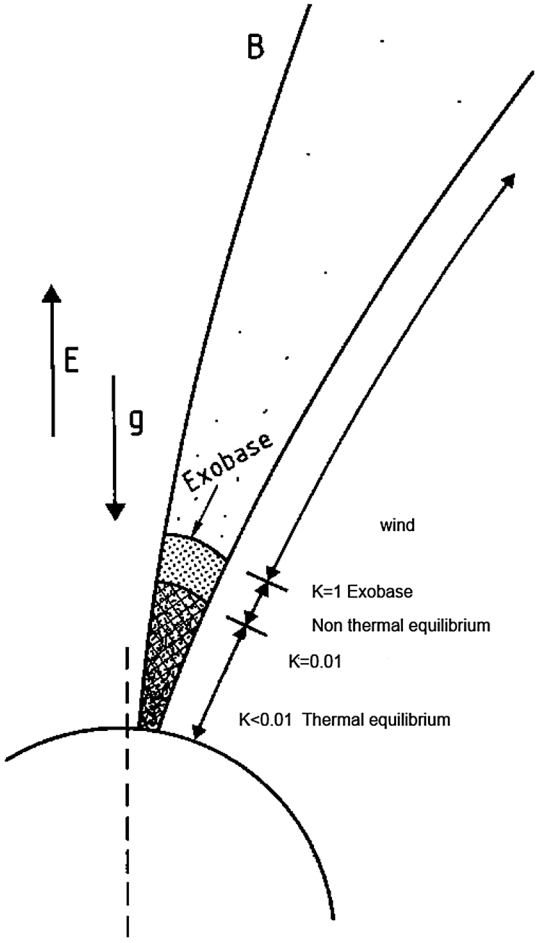

Figure 1. The different transition regions in a stellar ionized atmosphere.

velocity, the energetic particles are already collisionless at high altitudes, while the core of the distribution corresponding to the thermal particles continues to be submitted to collisions and remains close to a Maxwellian [*Pierrard et al*., 2011]. This nonthermal limit corresponds to the regions where the density becomes sufficiently low so that the Knudsen number $K_n > 0.01$ [*Scudder and Karimabadi*, 2013]. The Knudsen number is the ratio between the mean free path of the particles and the density-scale height.

The nonthermal level is well below the exobase, i.e., the altitude where the number of collisions becomes even lower so that a wind can escape from the atmosphere of a planet or a star. This level of the exobase is defined as the altitude where the Knudsen number $K_n = 1$. For the Sun, it corresponds to a radial distance around 1.5 and 2 R_S [*Lemaire and Pierrard*, 2001]. At this altitude, the diffusion due to the Coulomb collisions cannot keep the distributions isotropic anymore.

These two limits correspond to the regions where significant modifications appear in the plasma characteristics of the solar atmosphere (and more generally of all stellar atmospheres). The nonthermal limit can be identified to the top of the chromosphere. The exobase corresponds to the start of the solar wind expansion.

So in our model applied here to the solar corona and solar wind, we divide the transition region into two distinct levels as shown in Figure 1:

1. The nonthermal region, from the top of the chromosphere up to 2 R_S. In this region, the VDFs of all the particles are isotropic but non-Maxwellian. We assume that they are given by isotropic kappa distributions. Due to the Coulomb collision cross section, suprathermal particles are collisionless at very low altitudes. We consider that at the top of the chromosphere, all the particles have a kappa distribution with moderated kappa index ($\kappa = 5$) and the same temperature ($T_c = 10{,}000$ K). Note that the kappa index could be different for each particle species, but we use here the simplest assumptions.
2. The solar wind region above 2 R_S where the VDFs of the particles become anisotropic due to the decreasing Coulomb collisions. This is the beginning of the solar wind expansion (exobase at 2 R_S)

4. Coronal Heating

4.1. Temperature Increase Associated to the Presence of Suprathermal Particles

Kappa values obtained by fitting the observed electron VDF from Ulysses in the solar wind range between 2 and 7 [*Maksimovic et al*., 1997b]. The kappa fit parameters obtained in the slow-speed solar wind are a little bit larger than in the high-speed solar wind, suggesting a link between the velocity and the suprathermal electrons.

The energy contained in suprathermal tails causes an increase of the temperature into the transition region and low corona by velocity filtration, i.e., without any other addition of energy [*Scudder*, 1992b, 1992c]. Let us assume that at the top of the chromosphere, the plasma is in thermal equilibrium so that all the particles (electron, proton, and all ion species) have the same temperature of 10,000 K and that the Coulomb collisions are able to maintain isotropic distributions. Nevertheless, these collisions are not sufficient to

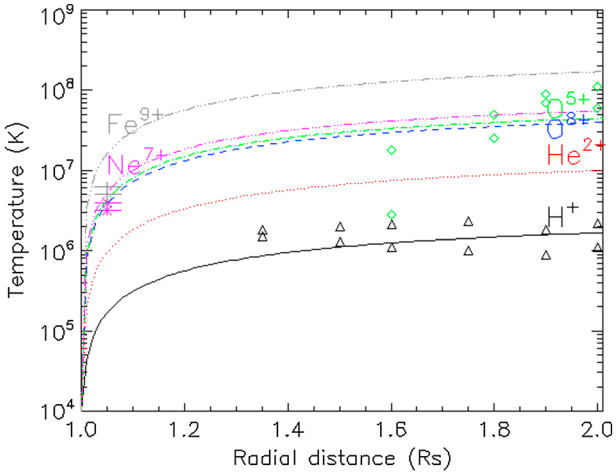

Figure 2. Temperature increase obtained in the solar corona when kappa distributions with $T_0 = 10{,}000$ K and kappa = 5 are assumed at the top of the chromosphere. The temperature profiles are compared to SOHO temperature observations.

maintain Maxwellian distributions at the top of the chromosphere, so that the distributions are given by kappa functions characterized by enhanced suprathermal tails. We take moderated tails simulated by a kappa index of 5. Note that in the solar wind, even lower values of kappa (corresponding to higher tails) are generally observed for the electrons [*Maksimovic et al.*, 1997b] and minor ions [*Collier et al.*, 1996], but at these low levels, the tails should be quite moderate due to Coulomb collisions being more abundant than at higher altitudes. Starting from such isotropic distributions at low altitude, we can obtain the kappa distributions at higher altitudes from the Liouville theorem and calculate the density and temperature profiles analytically. In contrast to a Maxwellian distribution for which the temperature remains constant, the temperature of the particles in an attractive potential with a kappa distribution increases with the radial distance following the law [*Scudder*, 1992b]:

$$T(r) = T(r_c)\left(1 + \frac{q(r)}{\kappa}\right) \tag{11}$$

where

$$q(r) = \frac{m\phi_g(r) + ZeV(r) - m\phi_g(r_c) - ZeV(r_c)}{kT_c} \tag{12}$$

$\phi_g(r)$ is the gravitational potential, $V(r)$ is the electrostatic potential, r_c corresponds to the top of the chromosphere, where $T(r_c) = 10{,}000$ K and $\kappa = 5$ for all the particles.

When kappa tends to infinity, we recover the Maxwellian isothermal property: $T = T(r_c)$.

Figure 2 illustrates the temperature increase obtained in the case $\kappa = 5$ for the different particles. Because the temperature and the kappa index are the same for electrons and protons, the electrostatic potential is given by the Pannekoek–*Rosseland* [1924] expression. This electrostatic potential ensures that the total potential (gravitational + electrostatic potential) is identical for the positive and negative charges so that the total density of the protons and other minor ions is everywhere equal to the density of the electrons.

The temperature increase is similar for electrons and protons that are the major species and mainly define the electrostatic potential. On the contrary, the minor ions have a higher temperature increase because the total potential q depends on the mass and the charge of the particles. Their density is negligible compared to that of the protons so that their influence on the electrostatic potential is very weak. The temperature increases with increasing mass per charge. It is mainly the gravitational potential that dominates at these low altitudes so that the temperature increase is proportional to the mass of the particles.

Figure 2 illustrates the temperature increase obtained for Fe^{9+} (gray), Ne^{7+} (magenta), O^{5+} (green), O^{8+} (blue), He^{2+} (red), and H^+ (black) and shows comparisons with temperature measurements deduced from SOHO (Solar Ultraviolet Measurements of Emitted Radiation and UltraViolet Coronagraph Spectrometer (UVCS)) [*Esser and Edgar*, 2000; *Tu et al.*, 1998]. The same colors are used for the respective ion measurements.

Note that this temperature increase is not just a property of the kappa distributions. It is a general property due to the presence of an enhanced population of suprathermal particles. The sum of two Maxwellians with different temperatures ($T_1 < T_2$) gives also an increase of the temperature, limited to the highest temperature T_2 [*Pierrard*, 2012c].

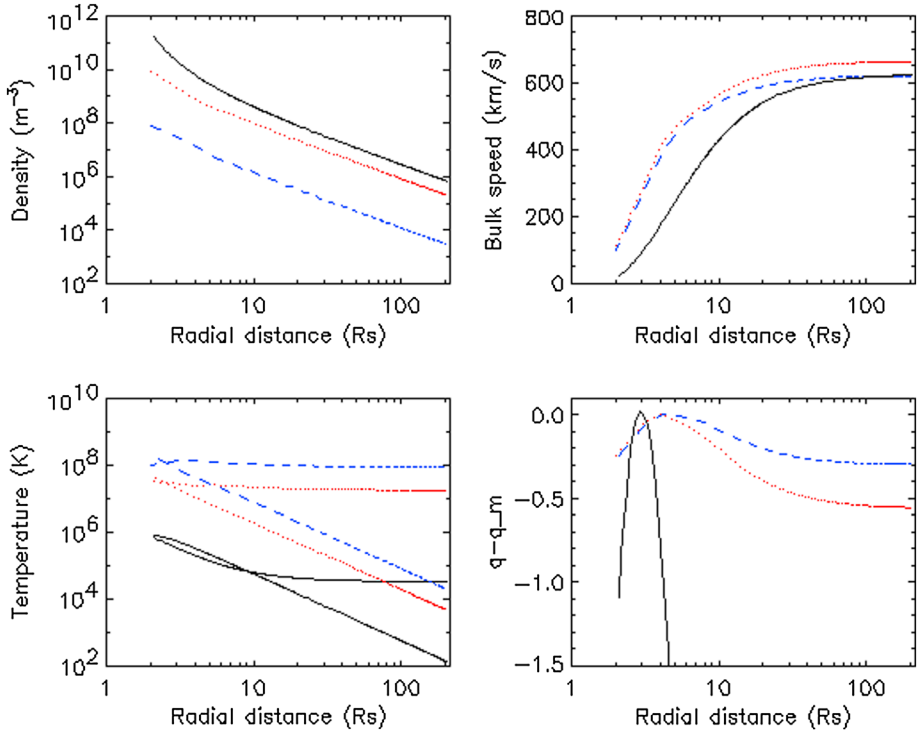

Figure 3. Radial profiles obtained for solar wind protons (black line), helium ions (red), and oxygen ions (blue) for the density, bulk velocity, temperatures, and total potential with the exospheric model for the electrons at the exobase level 2 R_S, where the temperature of the electrons and electrons is assumed to be $T_e = T_p = 10^6$ K.

4.2. Density Decrease

The density of the particles decreases with the altitude in the region above the chromosphere, following the analytical expression:

$$n(r) = n_c \left(1 + \frac{q(r)}{\kappa}\right)^{-\kappa+1/2}. \tag{13}$$

The density also decreases with altitude when kappa tends to infinity, i.e., for a Maxwellian:

$$n(r) = n_c \exp(-q(r)). \tag{14}$$

Again, because q depends on the mass and charge of the particles, the density of the heavy ions decreases faster than the density of the protons. At the top of the chromosphere, the ions are already ionized. Note that the density of the ions cannot be measured in the chromosphere, but they can be measured in the photosphere and in the solar wind [*Peter*, 2002].

5. The Solar Wind Expansion

Above a radial distance called the exobase corresponding to the regions where $K_n > 1$, the collisions between the particles can be neglected [*Lemaire and Scherer*, 1970]. This assumption corresponds to the exospheric approximation, where the right-hand side term in equation (1) is neglected; i.e., we assume that $(df/dt)_c = 0$. Note that the transition region between the collision-dominated region and the collisionless region has been studied in detail by solving the Fokker–Planck equation [*Pierrard et al.*, 2001c], but we consider here a model based on the simplest exospheric approximation since it provides analytical solutions of the Vlasov equation given by *Pierrard and Lemaire* [1996] for kappa distributions and by *Lamy et al.* [2003] for low exobase.

We do not repeat here these equations but only show the results in continuity of the coronal conditions. In this exospheric approximation, the VDFs of the particles become anisotropic, because particles with

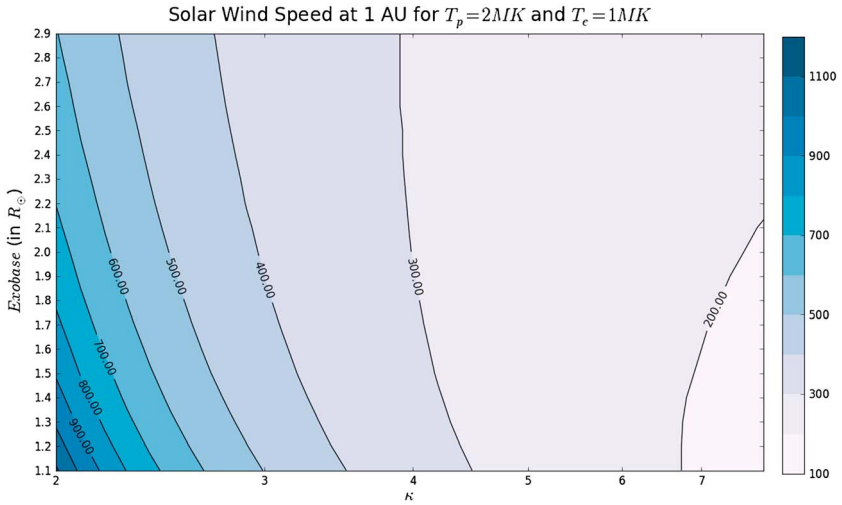

Figure 4. Bulk velocity at 1 AU (color scale in km/s) as a function of the exobase radial distance (vertical axis in solar radii) and of the kappa index (horizontal axis in logarithmic scale).

enough energy will escape to the interplanetary space and not come back to the Sun. Due to this anisotropy, there are more particles escaping than coming back to the Sun, and this effect generates the solar wind flux. We assume here the level of the exobase at 2 R_S and only electrons are assumed to have suprathermal tails, since it was shown that the suprathermal protons have only a minor influence [*Maksimovic et al.*, 2001].

Figure 3 shows typical radial profiles of the solar wind obtained with the exospheric model for the electrons at the exobase level 2 R_S, where the temperature of the electrons is assumed to be $T_e = T_p = 10^6$ K. It can be seen that the density continues to decrease, while the temperature reaches a maximum and begins to decrease. Note that the maximum of electron temperature is obtained around 2 R_S even when the exobase is located at lower altitudes, corresponding well to the temperature inversion profiles deduced from coronal observations during solar eclipses [*Pierrard et al.*, 2014].

The bulk velocity of the solar wind that was zero below the exobase increases very fast up to 10 R_S and then tends asymptotically to a constant value. The same bulk velocity is obtained for electrons and protons, but the bulk velocity of each ion species will depend on their mass, charge, and mainly on their temperature at the exobase.

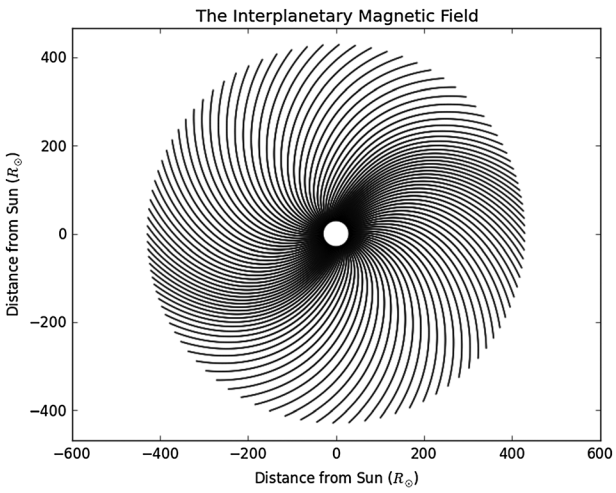

Figure 5. Magnetic field obtained with equations (15) to (18) with $\gamma = 0.01$.

Figure 3 (bottom right) represents $q - q_m$, the total potential normalized so that it is equal to zero at its maximum. The maximum corresponds to the region where the electrostatic force becomes larger than the attractive gravitational force. The temperature at 2 R_S is chosen to be 2.5×10^8 K for the oxygen ions, following UVCS measurements. T_{He} cannot be measured at 2 R_S, but we choose 5.7×10^7 K in this example. This value can be reached at 2 R_S by using the isotropic model with the assumption of a very low value of $\kappa = 2.1$. This example illustrates that the bulk velocity of the ions can be even larger than that of the other solar wind particles if their exobase temperature is sufficiently high.

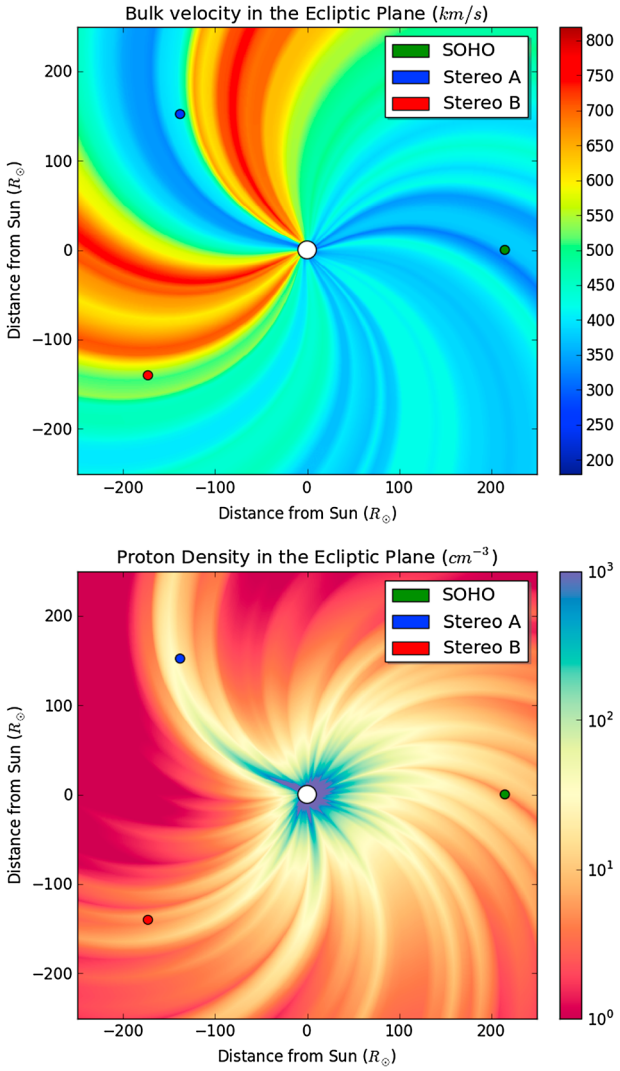

Figure 6. (top) Solar wind bulk velocity and (bottom) number density obtained in the ecliptic plane for CR2137 using the exospheric kappa model and ACE observations as boundary conditions.

The temperature of the minor ions is crucial for their acceleration in the exospheric model. The heavy ions can reach high bulk velocities at 1 AU only if their temperature in the corona is sufficiently high, because they have a large mass on charge ratio that attracts them more to the Sun than the protons. Very high ion temperatures in the solar corona are not unrealistic: their observations deduced from spectroscopy show indeed very high values [*Tu et al.*, 1998].

Note that the temperature obtained for the ions with the exospheric model is anisotropic at the exobase with $T_\perp > T_{//}$ due to the absence of incoming particles. The temperatures of the protons and of the oxygen ions are indeed observed to be anisotropic in the corona with even larger anisotropies that can reach 10–100 for $T_\perp/T_{//}$ for O^{5+} ions for instance (see *Cranmer* [2002] for a review of the high-speed solar wind characteristics). Such high anisotropies could be taken into account in the model by considering anisotropic bi-kappa distributions with different $T_{//}$ and $T_\perp$ already at the top of the chromosphere (see Appendix A). At higher radial distances, the opposite anisotropy is observed, i.e., $T_{//} > T_\perp$, as also obtained with the solar wind model due to the fast decrease of the perpendicular temperature. Note that while the global density, temperature, and bulk velocity profiles of the model reproduce well the solar wind observations, the temperature anisotropies and the heat flux are too large with the exospheric model at large radial distances, due to the assumption of a complete absence of interactions between the particles. Models including effects of Coulomb collisions and wave particle interactions like whistler [*Pierrard et al.*, 2011] and Alfvén waves [*Pierrard and Voitenko*, 2013] have also been developed by numerically solving the evolution equation. Their solutions show that these effects modify the pitch angle diffusion of the particles but not much the profiles of the average even moments.

In Figure 3, we assumed a low value of kappa ($\kappa = 2.5$) for the electrons to be able to reach high bulk velocities for the electrons and protons in the solar wind. Indeed, the suprathermal electrons determine the flux of escaping particles and accelerate the wind to high velocities when κ is small. The dependence of the final bulk velocity as a function of the kappa index and of the exobase altitude is illustrated in Figure 4.

The asymptotic wind speed is controlled by the suprathermal tail strength parameter [*Scudder*, 1992c]. Indeed, it can be seen that the bulk velocity reached at large radial distances is the highest when the exobase and the kappa index are the lowest. In Figure 4, $T_e = 10^6$ K and $T_p = 2\ 10^6$ K. Higher bulk velocities can even be reached by assuming a lower T_p. With $T_e = T_p = 10^6$ K and $r_0 = 1.1\ R_S$, the final bulk velocity can reach $v = 1470$ km/s for $\kappa = 2$.

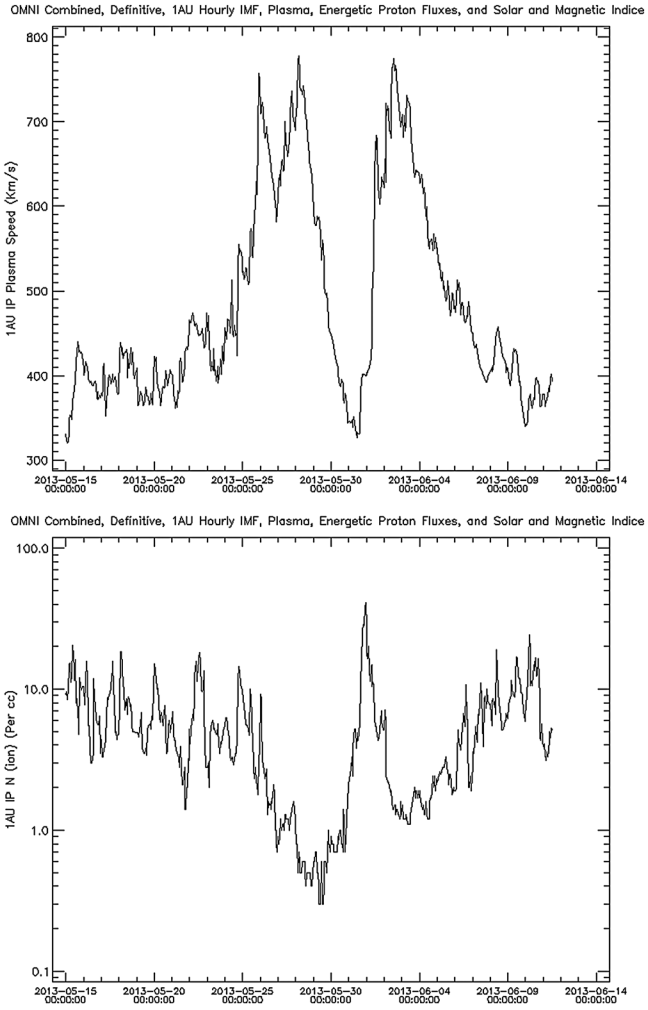

Figure 7. (top) Solar wind bulk velocity and (bottom) number density observed at 1 AU in the ecliptic plane for CR2137 from 15 May 2013 to 14 June 2013 by ACE.

6. Global Solar Wind Model

The model can be used to determine the characteristics of the plasma from low altitudes in the corona to large distances in the heliosphere. It is then necessary to know the densities and temperatures at a given reference altitude to determine the profiles at other distances. We could use conditions of density and temperature deduced in the corona from spectral observations at specific dates when available. But we only have access to magnetograms and empirical models obtained in the solar corona [*Lionello et al.*, 2001].

When suitable boundary conditions near the Sun are available, it is possible to implement the interactions of interplanetary streams. The theory behind magnetic fields of interplanetary streams have been studied in the past by several others. Most notably *Siscoe* [1970] and *Barouch and Burlaga* [1976] derived equations for the interplanetary magnetic field when the solar wind speed at the solar surface varies. In principle, these expressions make it possible to determine the magnetic field lines. Sadly, however, these mathematical expressions cannot be used because the derived fields are not divergence free.

So instead, an ad hoc magnetic field is constructed that hopefully will display the physical characteristics correctly and visualize the areas of compression and rarefaction (when the frozen-in condition is assumed).

$$r^2 B_r(r,\phi) = \left[u\left(\phi - \frac{\Omega(r-r_0)}{v_p}\right) - v_p\right] e^{-\gamma(r-r_0)} + v_p \tag{15}$$

$$r^2 B_\phi(r,\phi) = -\Omega(r-r_0)\left[1 - e^{-\gamma(r-r_0)}\left[\frac{\gamma}{\Omega}\left[\int u\left(\phi - \frac{\Omega(r-r_0)}{v_p}\right) - v_p d\phi\right] + \frac{1}{v_p}\left[u\left(\phi - \frac{\Omega(r-r_0)}{v_p}\right) - v_p\right]\right]\right]$$
$$v_p = \frac{1}{2\pi}\int_0^{2\pi} u(\phi_0) d\phi_0, \tag{16}$$

where $\Omega = 2.865 \times 10^{-6}$ rad/s is the angular velocity of the solar rotation, u is the velocity of the solar wind, and v_p is the velocity averaged on the azimuth ϕ in spherical coordinates.

These equations contain an analytical velocity function with a feedback loop. Also, an "air drag" coefficient γ is introduced to ensure that the initially varying solar wind speed $u(\phi_0)$ at the solar surface goes to a constant averaged value at farther distances. If the boundary conditions near the Sun are discrete, the analytical velocity function $u(\phi_0)$ can be determined by constructing a cubic spline through them.

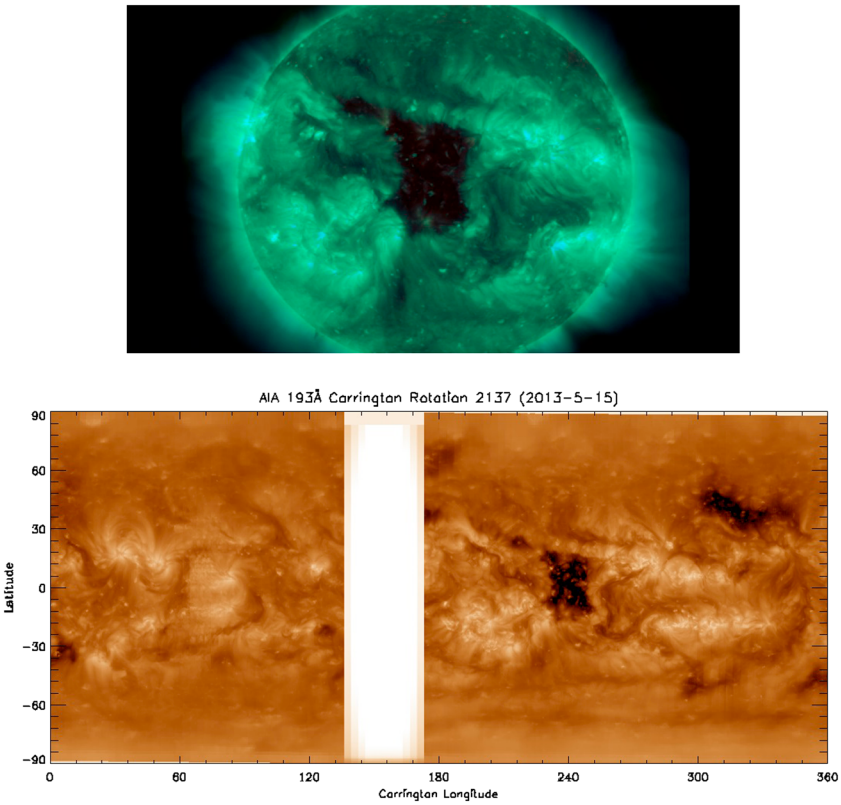

Figure 8. (top) Coronal holes observed on 30 May 2013 by SDO. (bottom) Brightness measured by the instrument Atmospheric Imaging Assembly at 193 Å. Unfortunately, some observations were not recorded during that particular Carrington rotation 2137.

The magnetic field lines can then be reconstructed by integrating the following equations with a fourth-order Runge–Kutta method:

$$\frac{rd\phi}{dr} = \frac{B_\phi}{B_r} = \frac{u_\phi}{u_r}, \tag{17}$$

where u_r and u_ϕ are, respectively, the radial and azimuthal velocity of the solar wind. As an example, we provide an analytical velocity profile capturing two high-speed streams in Figure 5:

$$u(\phi_0) = 450 + 250\cos(2\phi_0). \tag{18}$$

Since boundary conditions at 2.5 R_S are not available at the moment, we use in Figure 6 observations at 1 AU obtained from ACE spacecraft to model the characteristics of the plasma in the ecliptic plane assuming stationarity. Quasi-steady state is indeed often found during solar minimum activity when corotating interaction regions are observed during several Carrington rotations (CRs). Figures 6a and 6b show the bulk velocities and density obtained in the ecliptic plane for CR2137 when a coronal hole was observed in the direction of the Earth. Due to the solar rotation, the fluxes take the shape of a Parker spiral (with constant speed) to be taken into account in the kinetic model [*Pierrard et al.*, 2001a]:

$$r^2 B_r = r_0^2 B_0, \tag{19}$$

$$r^2 B_\phi = r_0^2 B_0 \frac{\Omega}{u_r}(r - r_0)\cos\lambda \tag{20}$$

where B_0 is the radial component of the magnetic field at the radial distance r_0 and λ is the heliographic latitude. The average speed of the Parker spiral is deduced by taking the average of the ACE solar wind speed data for CR2137.

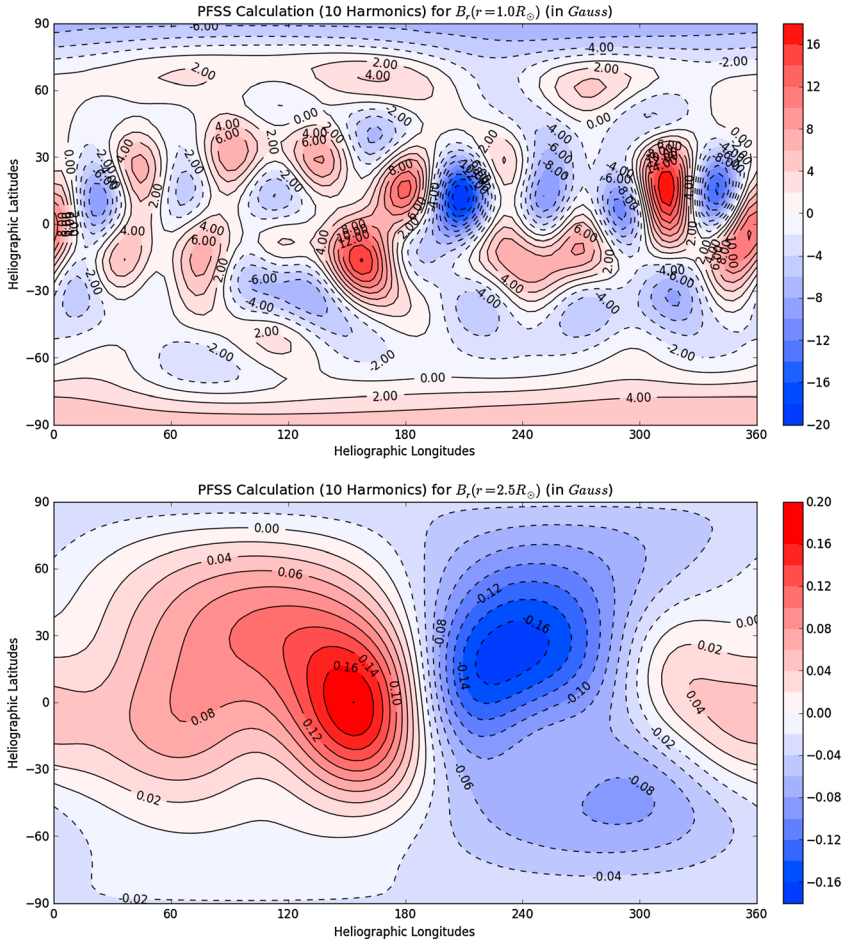

Figure 9. (top) Radial component of the photospheric magnetic field at 1 R_S. (bottom) Magnetic field at 2.5 R_S, where the field is considered fully radial and where it is dragged out by the solar wind.

These figures were obtained by using ACE observations of number density and bulk velocity as boundary conditions at 1 AU from 15 May 2013 to 14 June 2013. By this way, we can obtain a representation of the heliosphere and determine the solar wind characteristics in the acceleration region and more generally in regions lower than 0.3 AU, where no in situ observations are available [*Schwenn and Marsch*, 1991]. Future missions like Solar Orbiter and Solar Probe will give the opportunity to obtain observations closer to the Sun.

The bulk velocities and number densities observed by ACE at 1 AU and used as boundary conditions are represented in Figure 7. The kappa value for each flux tube is determined from the kappa model assuming an exobase at 2 R_S.

Two high-speed streams can be observed at that time that can be associated to the coronal holes observed in direction of the Earth by SDO (Solar Dynamics Observatory), as illustrated in Figure 8 by the darker regions in the equatorial plane of the Sun. These high-speed streams are associated to lower densities and temperatures in the corona. The same event has recently been studied by *Nikolic et al.* [2014].

The model can be used to make the link between the coronal and the solar wind observations, especially during CIR and/or when coronal holes are in the direction of the Earth.

For CR2137, we reconstructed the coronal magnetic field under the assumption that there are no currents running in the corona, obtaining the potential field source surface (PFSS) [*Altschuler and Newkirk*, 1969; *Hoeksema et al.*, 1983; *Wang and Sheeley*, 1990]. The source surface is taken at 2.5 R_S (as generally done) and the magnetic field is expanded up to 10 spherical harmonics. The spherical harmonic coefficients are taken from the GONG (Global Oscillation Network Group) observatory (gong.nso.edu).

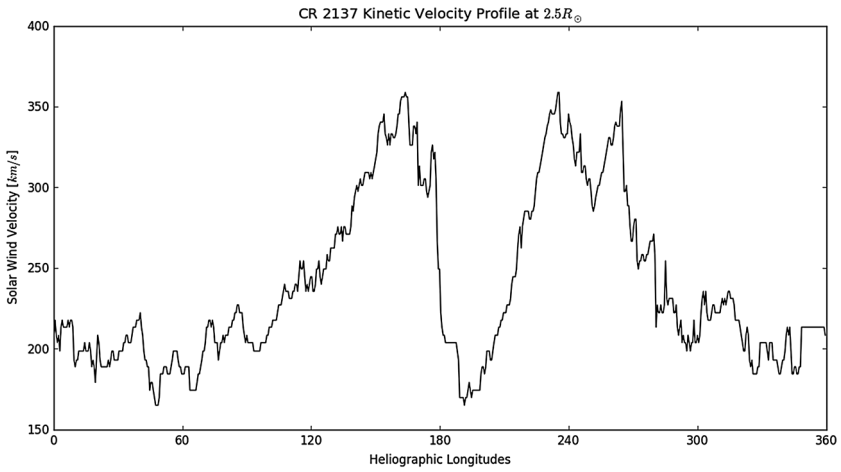

Figure 10. Bulk velocity obtained at 2.5 R_S with the exospheric model as a function of the heliographic longitudes.

Figure 9 (top) conveys the radial component of the photospheric magnetic field (at 1 R_S). During solar maximum, the number of sunspots is generally higher, leading to many strong localized magnetic field structures near the solar equator. Figure 9 (bottom) shows the magnetic field at 2.5 R_S, where the field is considered fully radial and where it is dragged out by the solar wind. The current sheet, the boundary layer between the two opposite polarities, takes on a very complex structure, very different from the dipole structure that one would expect during solar minimum.

The two major coronal holes during CR2137 seem to be connected to those areas (at 2.5 R_S) where there are strong radial magnetic fields.

Figure 10 shows the bulk velocity found at 2.5 R_S by using the kappa kinetic model and using the ACE observations at 1 AU as boundary conditions. One can clearly see that the two high-speed streams are associated to the two magnetic structures (red and blue) obtained from the PFSS in Figure 9. Note that the first high-speed stream arriving at the Earth (see Figure 7) originates from the coronal region located around 220° of heliographic longitude, and the second high-speed stream originates from the region around 150° of heliographic longitude.

7. Discussion

In fluid models, the spatial distributions of the macroscopic quantities (particle number density, velocity, and temperatures) are obtained by solving moment equations directly. As space plasmas deal with charged constituents, the required electromagnetic field information is determined by the Maxwell equations, which augment the moment equations. The moment equations themselves are in fact obtained by multiplying the kinetic Boltzmann equation governing the velocity distribution functions by various velocity moments and integrating over velocity space. The result is a hierarchy of coupled differential equations—the transport or fluid equations—which describe the spatiotemporal variation of the moments of the velocity distribution functions of the electron and ion species. In doing so, the detailed features of the microscopic velocity distribution function are lost. Indeed, there is an infinite variety of VDFs, which share the same values for their lowest-order moments but show important deviations in higher-order moments. Note that it was recently proved that the analytical solutions obtained with the exospheric solar wind model based on kappa distributions indeed fulfill the MHD equations.

More advanced moment descriptions may distinguish between the partial density of the electrons and different ion species, individual species bulk speeds, parallel and perpendicular temperatures, up to parallel and perpendicular heat flow tensor components, or even higher moments of the underlying velocity distribution function. These are only fully available from a kinetic approach. This concerns for instance the existence of non-Maxwellian features in the energy spectrum of particles or asymmetries in their pitch angle distributions. The inclusion of suprathermal particles in the tail of the distributions can then easily be investigated by using kappa distributions, so that the velocity filtration effect, the temperature inversion

ofthe solar atmosphere, the anticorrelation between the temperatures and the density, and the implications for the solar wind acceleration suggested by *Scudder* [1992a, 1992b] can be clearly obtained analytically. Just the presence of suprathermal particles can heat the corona and accelerate the solar wind to high bulk velocities without the need of any additional energy or wave. At the same time, those more realistic kinetic approaches have typically compromised on the significant work involved with handling the six-dimensional coordinate velocity phase space and have, e.g., reduced the modeling by assuming a 1-D analytically prescribed backbone magnetic field topology, such as a simple Parker spiral field [*Pierrard and Pieters*, 2014].

Global single-fluid MHD models for the solar corona and interplanetary space behavior for propagating coronal mass ejections are successfully used for modern space weather simulations, despite a sometimes complete lack on such higher moment information. We can attribute this to the fact that global MHD models in essence concentrate on incorporating the complexity of the magnetic topology in full three-dimensional (3-D) settings. There, in their most advanced variant, one solves the full system of MHD equations, using magnetic fields as well as the plasma moments (density, velocity, and temperature) to obtain a global steady state solar wind solution.

An example of recent sophisticated MHD solar wind modeling is provided by *Feng et al*. [2012]. These authors realized a full adaptive mesh refinement implementation for generating a quasi-steady global MHD solar wind model, covering regions up to 328 R_S, and demonstrated convincing comparisons with interplanetary observations. The main aspect of this model is the fact that the match between observations and models is largely achieved by a fine-tuned volumetric heating term in the energy equation. Similar global solar wind models have also used this approach, and it is important to note that they all remain in a single-fluid, even ideal MHD setting, leaving the "closure" to the underlying discretization errors and the parameterized heating and/or momentum deposition terms. More realistic treatments must therefore first incorporate well-founded prescriptions, coming from kinetic model inputs. Our guiding principle here is to improve our understanding of space plasma phenomena, especially for the solar wind realms, by relating MHD and kinetic models, ultimately leading up to more realistic multiscale treatments.

The kinetic exospheric model has the advantage to be fully analytic. Its strong assumptions make it a first approximation model, but the averaged moments can be used for space weather predictions because they do not require long CPU time. The inclusion of the different interaction processes leads to the development of successive generations of more sophisticated kinetic models based on the solution of the Fokker–Planck equation including the effects of Coulomb collisions, turbulence, and kinetic Alfvén waves [*Pierrard*, 2012a]. These effects modify the VDF but not the averaged lowest moments of the particles, so that the simple analytical exospheric model can be used for space weather predictions.

8. Conclusions

In the present work, we show how the kappa distribution functions, as initially proposed by *Scudder* [1992a, 1992b], can be used to simulate the particles in the solar corona and the solar wind. The particles are characterized by an enhanced population of energetic particles in the tail of the distributions that has important consequences concerning the heating of the corona and the acceleration of the solar wind particles, for electrons, protons, and minor ions.

The model is based on the assumption that an enhanced population of suprathermal particles is present at the top of the chromosphere or at least at the exobase. Such suprathermal particles are in any case observed in many space plasmas and specifically at 1 AU in situ in the solar wind. Stationary states out of thermal equilibrium are frequently observed in space plasmas and can be simulated by using the kappa VDF. The coronal heating and solar wind acceleration are obtained to be natural consequences of the presence of these suprathermal particles, as it can be successfully described by using kappa VDF in an analytic model. In the present work, we extended the solar wind model developed on the basis of such kappa distributions by incorporating azimuthally varying 1 AU boundary conditions to produce a spatially structured view of the solar wind expansion. We illustrate the results of the model in two dimensions for a typical case when a clear connection can be obtained between the high-speed streams observed at 1 AU and the coronal holes which are sources of strong radial magnetic fields. A possible form of modified Parker spiral is suggested to take into account the dynamics of high-speed and slow-speed streams in azimuth.

Appendix A: Anisotropic Bi-Kappa Ion Distributions

VDF of ions with high thermal anisotropy can be simulated with bi-kappa (by analogy to bi-Maxwellian) distributions [*Summers and Thorne*, 1992]:

$$f = \frac{n}{\pi^{3/2}} \frac{1}{\theta_\perp^2 \theta_{//}} \frac{1}{\kappa^{3/2}} \frac{\Gamma(\kappa+1)}{\Gamma(\kappa-1/2)} \left(1 + \frac{v_{//}^2(r)}{\kappa\theta_{//}^2} + \frac{v_\perp^2(r)}{\kappa\theta_\perp^2}\right)^{-\kappa-1}$$

with $\theta_\perp^2 = \frac{\kappa-3/2}{\kappa}\frac{2kT_\perp}{m}$ and $\theta_{//}^2 = \frac{\kappa-3/2}{\kappa}\frac{2kT_{//}}{m}$.

In this case, applying Liouville's theorem with the conservation of energy and magnetic moment, the temperature increase is analytically obtained by

$$T_{//}(r) = T_{//}(r_0)\left(1 + \frac{2\phi(r)}{\kappa m\theta_{//}^2}\right)$$

$$T_\perp(r) = T_\perp(r_0)\left(1 + \frac{2\phi(r)}{\kappa m\theta_{//}^2}\right) \frac{1}{\frac{T_{0\perp}}{T_{0//}} + \left(1 - \frac{T_{0\perp}}{T_{0//}}\right)\frac{B_0}{B}}$$

where ϕ is the potential. Note that the parallel temperature is not affected by the anisotropy, while the perpendicular one is with a variation depending on the magnetic field strength.

The density decrease is given by

$$n(r) = n(r_0)\left(1 + \frac{2\phi(r)}{\kappa m\theta_{//}^2}\right)^{-\kappa+1/2} \frac{1}{\frac{T_{0\perp}}{T_{0//}} + \left(1 - \frac{T_{0\perp}}{T_{0//}}\right)\frac{B_0}{B}}$$

Assuming such anisotropic temperatures for the heavy ions in the solar corona, as the spectral observations seem to indicate, leads to more realistic temperature anisotropies at large distances as well.

Acknowledgments

The exospheric solar wind model developed at the Belgian Institute for Space Aeronomy and used in the present work can be run on request on the Community Coordinated Modeling Center website of NASA (ccmc.gsfc.nasa.gov). The ACE data used as boundary conditions in Figure 7 are accessible on SPENVIS (www.spenvis.oma.be). The GONG model used in Figure 9 is accessible on gong.nso.edu. The research leading to these results has received funding from the Belgian Federal Science Policy in the framework of the program Interuniversity Attraction Pole for the project P7/08 CHARM. V. Pierrard thanks the STCE (Solar-Terrestrial Centre of Excellence) and BISA for their support.

Yuming Wang thanks Oleg Pokhotelov and another reviewer for their assistance in evaluating this paper.

References

Altschuler, M. D., and G. Newkirk (1969), Magnetic Fields and the Structure of the Solar Corona, *Sol. Phys.*, *9*, 131–149.

Barouch, E., and L. F. Burlaga (1976), Three-dimensional interplanetary stream magnetism and energetic particle motion, *J. Geophys. Res.*, *81*(13), 2103–2110, doi:10.1029/JA081i013p02103.

Collier, M. C., D. C. Hamilton, G. Gloeckler, P. Bochsler, and R. B. Sheldon (1996), Neon-20, Oxygen-16, and Helium-4 densities, temperatures, and suprathermal tails in the solar wind determined by WIND/MASS, *Geophys. Res. Lett.*, *23*, 1191–1194, doi:10.1029/96GL00621.

Cranmer, S. R. (2002), Coronal holes and the high-speed solar wind, *Space Sci. Rev.*, *101*, 229–294.

Esser, R., and R. J. Edgar (2000), Reconciling spectroscopic electron temperature measurements in the solar corona with in-situ charge state observations, *Astrophys. J. Lett.*, *532*, L71–74.

Feng, X., L. Yang, C. Xiang, C. Jiang, X. Ma, S. T. Wu, D. K. Zhong, and Y. Zhou (2012), Validation of the 3D AMR SIP-CESE Solar Wind Model for Four Carrington Rotations, *Sol. Phys.*, *279*, 207–229.

Hoeksema, J. T., J. M. Wilcox, and P. H. Scherrer (1983), The structure of the heliospheric current sheet: 1978–1982, *J. Geophys. Res.*, *88*, 9910–9918, doi:10.1029/JA088iA12p09910.

Khazanov, G. V., M. W. Liemohn, J. U. Kozyra, and T. E. Moore (1998), Inner magnetospheric superthermal electron transport: Photoelectron and plasma sheet electron sources, *J. Geophys. Res.*, *103*, 23,485–23,501, doi:10.1029/98JA02291.

Lamy, H., V. Pierrard, M. Maksimovic, and J. Lemaire (2003), A kinetic exospheric model of the solar wind with a non monotonic potential energy for the protons, *J. Geophys. Res.*, *108*, 1047–1057, doi:10.1029/2002JA009487.

Lemaire, J., and M. Scherer (1970), Model of the polar ion-exosphere, *Planet. Space Sci.*, *18*, 103–120.

Lemaire, J., and V. Pierrard (2001), Kinetic models of solar and polar winds, *Astrophys. Space Sci.*, *277*(2), 169–180.

Leubner, M. P. (2002), A nonextensive entropy approach to kappa distributions, *Astrophys. Space Sci.*, *282*, 573–579, doi:10.1023/A:1020990413487.

Liemohn, M. W., and G. V. Khazanov (1998), Collisionless plasma modeling in an arbitrary potential energy distribution, *Phys. Plasmas*, *5*, 580–589.

Lionello, R., J. A. Linker, and Z. Mikic (2001), Including the transition region in models of the large-scale solar corona, *Astrophys. J.*, *546*, 542–551.

Livadiotis, G., and D. J. McComas (2009), Beyond kappa distributions: Exploiting Tsallis statistical mechanics in space plasmas, *J. Geophys. Res.*, *114*, A11105, doi:10.1029/2009JA014352.

Livadiotis, G., and D. J. McComas (2010), Exploring transitions of space plasmas out of equilibrium, *Astrophys. J.*, *714*, 971–987, doi:10.1088/0004-637X/714/1/971.

Livadiotis, G., and D. J. McComas (2011), Invariant Kappa distribution in space plasmas out of equilibrium, *Astrophys. J.*, *741*(88), 28, doi:10.1088/0004-637X/741/88.

Maksimovic, M., V. Pierrard, and J. Lemaire (1997a), A kinetic model of the solar wind with Kappa distributions in the corona, *Astron. Astrophys.*, *324*, 725–734.

Maksimovic, M., V. Pierrard, and P. Riley (1997b), Ulysses electron distributions fitted with Kappa functions, *Geophys. Res. Lett.*, *24*(9), 1151–1154, doi:10.1029/97GL00992.

Maksimovic, M., V. Pierrard, and J. Lemaire (2001), On the exospheric approach for the solar wind acceleration, *Astrophys. Space Sci.*, *277*(2), 181–187.

Meyer-Vernet, N., M. Moncuquet, and S. Hoang (1995), Temperature inversion in the Io plasma torus, *Icarus*, *116*, 202.
Nikolic, L., L. Trichtchenko, and D. Botler (2014), A numerical framework for operational solar wind prediction, *Plasma Fusion Res.*, *9*, 1–5, doi:10.1585/pfr.9.3406099.
Peter, H. (2002), Composition of the solar chromosphere and transition region, *Adv. Space Res.*, *30*, 13–22.
Pierrard, V. (2009), Kinetic models for the exospheres of Jupiter and Saturn, *Planet. Space Sci.*, *57*, 1260–1267, doi:10.1016/j.pss.2009.04.011.
Pierrard V. (2012a), Kinetic models for solar wind electrons, protons and ions, chapter in "*Exploring the solar wind*", edited by M. Lazar, pp. 221-240, Intech., Rijeka, Croatia.
Pierrard, V. (2012b), Solar wind electron transport: interplanetary electric field and heat conduction, *Space Sci. Rev. (solar wind)*, doi:10.1007/s11214-011-9743-6.
Pierrard, V. (2012c), Effects of suprathermal particles in space plasmas, ICNS Annual International Astrophysics Conference, *Proc. Am. Inst. Phys.*, *1436*, 61–66, doi:10.1063/1.4723591.
Pierrard, V., and K. Borremans (2012a), The ionosphere coupled to the plasmasphere and polar wind models, in *Numerical Modeling of Space Plasma Flows: Astronum-2011*, *Astron. Soc. Pacific Conf. Ser.*, vol. 459, edited by N. V. Pogorelov et al., pp. 234–239, San Francisco, Calif.
Pierrard, V., and K. Borremans (2012b), Fitting the AP8 spectra to determine the proton momentum distribution functions in space radiations, *Radiat. Meas.*, *47*, 401–405, doi:10.1016/j.radmeas.2012.04.002.
Pierrard, V., and H. Lamy (2003), The effects of the velocity filtration mechanism on the minor ions of the corona, *Sol. Phys.*, *216*, 47–58.
Pierrard, V., and M. Lazar (2010), Kappa distributions: Theory and applications in space plasmas, *Sol. Phys.*, *287*, 153–174, doi:10.1007/s11207-010-9640-2.
Pierrard, V., and J. Lemaire (1996), Lorentzian ion exosphere model, *J. Geophys. Res.*, *101*, 7923–7934, doi:10.1029/95JA03802.
Pierrard, V., and J. Lemaire (2001), Exospheric model of the plasmasphere, *J. Atmos. Sol. Terr. Phys.*, *63*(11), 1261–1265.
Pierrard, V., and M. Pieters (2014), Toward a 3D kinetic model of the solar wind, in *Outstanding Problems in Heliophysics: From Coronal Heating to the Edge of the Heliosphere*, *Astron. Soc. Pacific Conf. Ser.*, vol. 484, edited by Q. Hu and G. P. Zank, pp. 167–172, San Francisco, Calif.
Pierrard, V., and Y. Voitenko (2013), Modification of the proton velocity distributions by Alfvénic turbulence in the solar wind, *Sol. Phys.*, *288*(1), 355–368, doi:10.1007/s11207-013-0294-8.
Pierrard, V., K. Issautier, N. Meyer-Vernet, and J. Lemaire (2001a), Collisionless solar wind in a spiral magnetic field, *Geophys. Res. Lett.*, *28*, 223–226, doi:10.1029/2000GL011888.
Pierrard, V., M. Maksimovic, and J. Lemaire (2001b), Self-consistent kinetic model of solar wind electrons, *J. Geophys. Res.*, *107*, 29,305–29,312, doi:10.1029/2001JA900133.
Pierrard, V., M. Maksimovic, and J. Lemaire (2001c), Core, halo and strahl electrons in the solar wind, *Astrophys. Space Sci.*, *277*(2), 195–200.
Pierrard, V., H. Lamy, and J. Lemaire (2004), Exospheric distributions of minor ions in the solar wind, *J. Geophys. Res.*, *109*, A02118, doi:10.1029/2003JA010069.
Pierrard V., G. V. Khazanov, and J. Lemaire (2007), Current-voltage relationship, *J. Atmos. Sol. Terr. Phys.*, *69*(12), Recent Advances in the Polar Wind Theories and Observations, 2048-2057, guest editors: Tam, Pierrard and Schunk, doi:10.1016/j.jastp.2007.08.005.
Pierrard, V., M. Lazar, and R. Schlickeiser (2011), Evolution of the electron distribution function in the wave turbulence of the solar wind, *Sol. Phys.*, *269*(2), 421–438, doi:10.1007/s11207-010-9700-7.
Pierrard, V., J. F. Lemaire, K. Stegen, and K. Borremans (2014), Coronal temperature profiles obtained from kinetic models and from coronal brightness measurements obtained during solar eclipses, *Sol. Phys.*, *289*, 183–192, doi:10.1007/S11207-013-0320-x.
Rosseland, S. (1924), Electrical state of a star, Monthly Notices, *Royal Astron. Soc.*, *84*, 720–728.
Schwenn, R., and E. Marsch (1991), *Physics of the Inner Heliosphere*, Springer, New York.
Scudder, J. D. (1992a), On the causes of temperature change in homogeneous low-density astrophysical plasmas, *The Astrophys. J.*, *398*, 299–318.
Scudder, J. D. (1992b), Why all stars possess circumstellar temperature inversions, *The Astrophys. J.*, *398*, 319–349.
Scudder, J. D. (1992c), The cause of the coronal temperature inversion of the solar atmosphere and the implications for the solar wind, in *Solar Wind Sven*, edited by E. Marsch and R. Schwenn, pp. 103–112, Pergamon Press, Oxford, U. K.
Scudder, J. D., and H. Karimabadi (2013), Ubiquitous non-thermals in astrophysical plasmas: Restating the difficulty of maintaining Maxwellians, 770, 11.
Scudder, J. D., and S. Olbert (1979), A theory of local and global processes which affect solar wind electrons: The origin of typical 1 AU velocity distribution functions – Steady state theory, *J. Geophys. Res.*, *84*, 2755–2772, doi:10.1029/JA084iA06p02755.
Siscoe, G. L. (1970), Fluid dynamics of thin solar wind filaments, *Sol. Phys.*, *13*, 490–498.
Summers, D., and R. M. Thorne (1992), A new tool for analyzing microinstabilities in space plasma modeled by a generalized Lorentzian (kappa) distribution, *J. Geophys. Res.*, *97*, 16,827–16,832, doi:10.1029/92JA01664.
Tam, S. W. Y., T. Chang, and V. Pierrard (2007), Kinetic modeling of the polar wind, *J. Atmos. Sol. Terr. Phys.*, *69*(16), 1984–2027, doi:10.1016/j.jastp.2007.08.006.
Tu, C.-Y., E. Marsch, K. Wilhelm, and W. Curdt (1998), Ion temperatures in a solar polar coronal hole observed by SUMER on SOHO, *Astrophys. J.*, *503*, 475–382.
Wang, Y.-M., and N. R. Sheeley Jr. (1990), Magnetic flux transport and the sunspot-cycle evolution of coronal holes and their wind streams, *Astrophys. J.*, *365*, 372–386.
Zouganelis, I., M. Maksimovic, N. Meyer-Vernet, H. Lamy, and V. Pierrard (2003), A new exospheric model of the solar wind acceleration: The transsonic solutions, CP679, in *Solar Wind Ten Proc*, edited by M. Velli, R. Bruno, and F. Malara, pp. 315–318, American Institute of Physics, New York.